Polyanionic ligand platforms for methyl- and dimethylaluminum arrays.

Philip I. Richards, Gavin T. Lawson, Jamie F. Bickley, Craig M. Robertson, Jonathan A. Iggo and Alexander Steiner*

Department of Chemistry, University of Liverpool, Crown Street, Liverpool, L69 7ZD, U.K.

Supporting Information Placeholder

ABSTRACT: Trimethylaluminum finds widespread applications in chemical and materials synthesis, most prominently in its partially hydrolyzed form of methylalumoxane (MAO) which is used as a co-catalyst in the polymerization of olefins. This work investigates the sequential reactions of trimethylaluminum with hexaprotic phosphazenes $(RNH)_6P_3N_3$ (= **X**H_6) equipped with substituents R of varied steric bulk including tert-butyl (**1**H_6), cyclohexyl (**2**H_6), isopropyl (**3**H_6), isobutyl (**4**H_6), ethyl (**5**H_6), propyl (**6**H_6), methyl (**7**H_6) and benzyl (**8**H_6). Similar to MAO, the resulting complexes of polyanionic phosphazenates $[\mathbf{X}H_n]^{n-6}$ accommodate multinuclear arrays of $[AlMe_2]^+$ and $[AlMe]^{2+}$. Reactions were monitored by ^{31}P NMR spectroscopy and structures were determined by single crystal X-ray diffraction. They included **1**$H_4(AlMe_2)_2$, **1**$H_3(AlMe_2)_3$, **2**$H_3(AlMe_2)_3$, **3**$(AlMe_2)_4AlMe$, **4**$H(AlMe_2)_5$, **4**$(AlMe_2)_6$, {**5**$H(AlMe_2)_4\}_2AlMe$, **5**$(AlMe_2)_6$, **6**$(AlMe_2)_6$, {**7**$(AlMe_2)_4AlMe\}_2$ and **8**$(AlMe_2)_6$. The study shows that subtle variations of the steric properties of the R-groups influence reaction pathways, levels of aggregation and fluxional behavior. While $[AlMe_2]^+$ is the primary product of the metalation, $[AlMe]^{2+}$ is utilized to alleviate overcrowding or to aid aggregation. At the later stages of metalation $[AlMe_2]^+$ groups start to scramble around congested sites. The ligands proved to be very robust and extremely flexible offering a unique platform to study complex multinuclear metal arrangements.

INTRODUCTION

Polyanionic phosphazenates are multi-site ligands that can accommodate arrays of metal centers.[1-3] They are obtained via deprotonation of hexaprotic cyclotriphosphazenes $(RNH)_6P_3N_3$ (labelled **X**H_6 hereafter).[4-6] The steric and electronic properties of the R-groups in the ligand periphery control the size and the layout of the coordinated arrangement.[7-9] The routes along which metalations can progress are manifold considering the large number of partially deprotonated ligand isomers that can exist (see Scheme 1). Nonetheless, metalations often proceed along distinctive pathways; for example reactions with butyllithium advance via the trianionic C_{3v}-symmetric isomer $[\mathbf{X}'''H_3]^{3-}$ which distributes its negative charge most effectively.[10-12]

This work explores the metalation of **X**H_6 with trimethylaluminum, a reagent that is widely applied in chemical and materials synthesis. It is a precursor for mono- and dimethylaluminum complexes that serve as catalysts in organic transformations.[13-19] The most prominent example is perhaps methylalumoxane (MAO), an ill-defined compound generated by controlled hydrolysis of $AlMe_3$ which is used as a co-catalyst in the polymerization of olefins.[20-25]. Trimethylaluminum is also an important precursor for the deposition of aluminum oxide and nitride layers which find applications as insulators and large band-gap semiconductors.[26-29]

Aggregates of organoaluminum oxides, hydroxides, amides and imides have been investigated in great detail, either as models for the structure of MAO or as precursors for chemical vapor deposition. As a result, a variety of cyclic and cage-like structures have been uncovered.[30-33] The few reports of multinuclear organoaluminum arrays that are supported by single multi-site ligands are limited to complexes of calixarenes, in which the metals are clustered around the rim of phenolate-O centers.[34,35]

We were interested how arrays of $[AlMe_2]^+$ and $[AlMe]^{2+}$ behave when assembled around polyanionic phosphazenate ligands and how the steric factor of the ligand affects the modes of coordination and levels of metalation. To shed light on this we investigated sequential reactions of trimethylaluminum with phosphazenes **X**H_6 equipped with different sized R groups and analyzed metalation pathways, coordination patterns and dynamic behavior of the resulting complexes.

RESULTS

The phosphazenes **X**H_6 used in this study included tert-butyl (**1**H_6), cyclohexyl (**2**H_6), isopropyl (**3**H_6), isobutyl (**4**H_6), ethyl (**5**H_6), propyl (**6**H_6), methyl (**7**H_6) and benzyl (**8**H_6) derivatives. Apart from **5**H_6 the syntheses of these were reported previously.[36] Metalations were conducted by stepwise addition of aliquots of trimethylaluminum in hexane at room temperature. If full deprotonation of the ligand was not achieved under these conditions the mixtures were heated to reflux. The reactions were followed by $^{31}P\{^1H\}$ NMR spectroscopy (Figure 1 shows the spectra of the sequential addition of $AlMe_3$ to **5**H_6). It signals molecular symmetry thanks to the characteristic coupling patterns of the three ^{31}P nuclei in the phosphazene ring: a set of three equivalent nuclei yields a singlet, two equivalent nuclei generate a doublet and a triplet (AX_2) while three inequivalent nuclei show three doublets of doublets

(AMX). If the spectra indicated the presence of a single product then crystallization trials were set up to grow crystals suitable for X-ray structure analysis. The crystal structures are presented in Figure 2 while Chart 1 displays the types of chelation found in them. Scheme 2 lists the complexes encountered in this study. Further spectra of sequential additions and variable temperature runs can be found in the ESI alongside crystallographic data.

Scheme 1. Map of deprotonation pathways between ligand isomers ($[X'H_4]^{2-}$, $[X''H_3]^{3-}$ and $[X'H_2]^{4-}$ are chiral; only one enantiomer is shown)

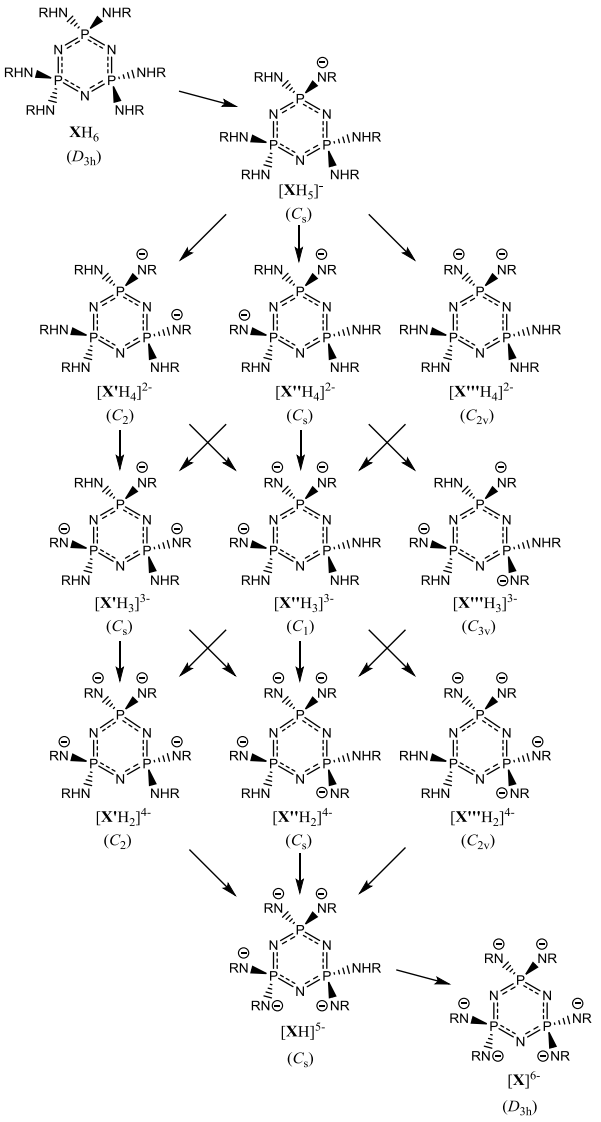

The first distinctive product forms after addition of two equivalents $AlMe_3$ at room temperature to $\mathbf{1}H_6$, $\mathbf{2}H_6$, $\mathbf{3}H_6$ and $\mathbf{4}H_6$, respectively. $^{31}P\{^1H\}$ NMR spectra of reaction solutions show an AX_2 set of signals indicating the equivalence of two P-nuclei in the phosphazene ring. Crystals suitable for X-ray analysis were obtained of the tert-butyl derivative. The crystal structure consists of the C_2 symmetric complex $\mathbf{1}'H_4(AlMe_2)_2$. It contains the dianionic ligand isomer $[\mathbf{X}'H_4]^{2-}$ featuring two deprotonated N(exo) sites positioned in non-geminal *trans*-configuration. The two $[AlMe_2]^+$ groups occupy bidentate chelates of type **I** located at opposite sides of the phosphazene ring.

After addition of three equivalents $AlMe_3$ at room temperature the ^{31}P NMR spectra of $\mathbf{2}H_6$ and $\mathbf{3}H_6$ show one AMX set. The crystals of the corresponding cyclohexyl derivative contain the complex $\mathbf{2}'H_3(AlMe_2)_3$. The trianionic ligand isomer $[\mathbf{X}'H_3]^{3-}$ distributes its three deprotonated N-sites in non-geminal *cis-trans* fashion. It accommodates the three $[AlMe_2]^+$ groups in separate bidentate type **I** chelates which breaks the C_s symmetry of the ligand yielding three unique phosphorus environments in agreement with the observed AMX pattern. Addition of three equivalents $AlMe_3$ to $\mathbf{4}H_6$, $\mathbf{5}H_6$ and $\mathbf{6}H_6$ at room temperature generates two sets of AMX signals. Attempts to separate the two species were unsuccessful. The only two isomers of $\mathbf{X}H_3(AlMe_2)_3$ that are compatible with AMX pattern in the $^{31}P\{^1H\}$ NMR spectra while also providing three separate type **I** sites are the asymmetric complexes $\mathbf{X}'H_3(AlMe_2)_3$ and $\mathbf{X}''H_3(AlMe_2)_3$. The reaction of $\mathbf{1}H_6$ with $AlMe_3$ advances beyond the dianionic stage only after prolonged heating. Refluxing a mixture with three of more equivalents $AlMe_3$ gives a single product that exhibits an AMX signal pattern similar to those observed for $\mathbf{2}'H_3(AlMe_2)_3$ and $\mathbf{3}'H_3(AlMe_2)_3$. Crystals of $\mathbf{1}'H_3(AlMe_2)_3$ show a coordination pattern analogous to $\mathbf{2}'H_3(AlMe_2)_3$.

Metalations of $\mathbf{2}H_6$ and $\mathbf{3}H_6$ progress beyond the trianionic ligand stage only after continuous heating. Refluxing reaction mixtures containing more than three equivalents $AlMe_3$ generates AMX sets that become the sole species with five or more equivalents. The crystal structure of the isopropyl derivative exhibits the complex $\mathbf{3}(AlMe_2)_4AlMe$ featuring a fully deprotonated phosphazenate ligand $[\mathbf{3}]^{6-}$. It retains the three chelates found in $\mathbf{X}'H_3(AlMe_2)_3$, while the fourth $[AlMe_2]^+$ group is accommodated in a bidentate chelate of type **II**. The $[AlMe]^{2+}$ unit, formally the product of twofold deprotonation, occupies a tridentate type **IV** chelate.

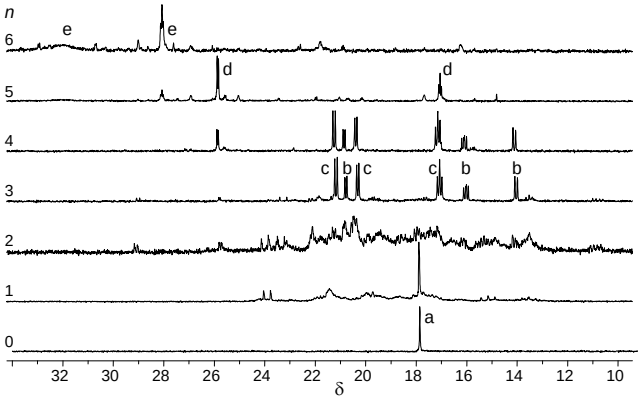

Figure 1. $^{31}P\{^1H\}$ NMR spectra of the sequential addition of *n* equivalents $AlMe_3$ to $\mathbf{5}H_6$ in hexane at room temperature. Species detected along the metalation pathway include $\mathbf{5}H_6$ (a), $\mathbf{5}'H_3(AlMe_2)_3$ (b), $\mathbf{5}''H_3(AlMe_2)_3$ (c), $\mathbf{5}H(AlMe_2)_5$ (d), $\mathbf{5}(AlMe_2)_6$ (e). Reactions with $n = 2$ yielded only turbid mixtures.

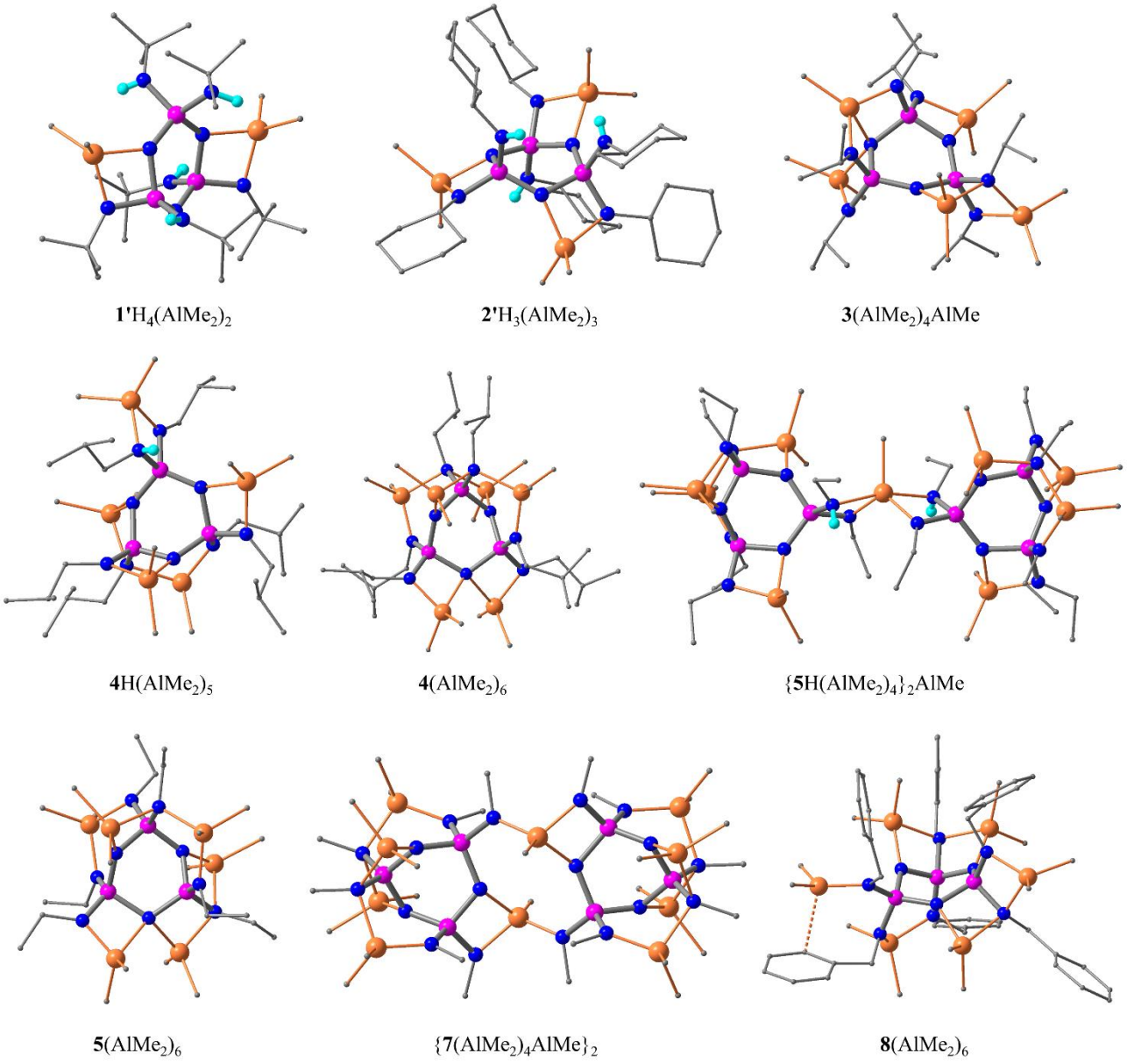

Figure 2. X-ray crystal structures (Al, orange; N, blue; P, purple; H, turquoise; C, grey; C-bound H-atoms are omitted for clarity).

Chart 1. Types of chelates coordinating $[AlMe_2]^+$ and $[AlMe]^{2+}$ groups, respectively.

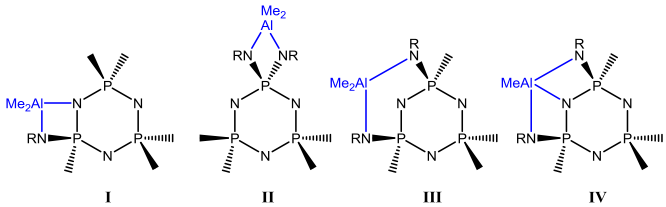

Scheme 2. Species observed along metalation routes (crystallographically characterized complexes are marked with an asterisk).

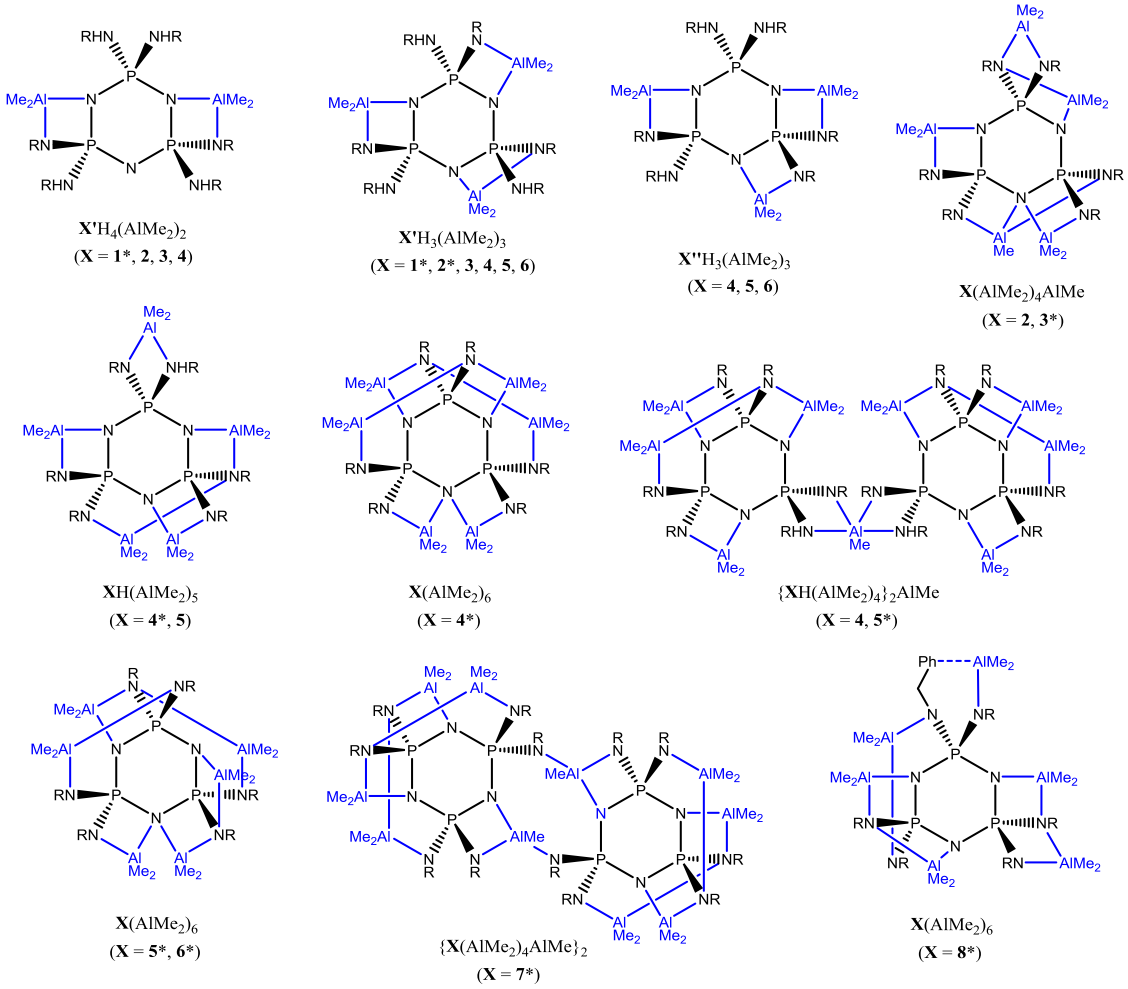

Addition of five equivalents $AlMe_3$ to **4**H_6 and **5**H_6 at room temperature gives rise to an AX_2 set in the $^{31}P\{^1H\}$ NMR spectra. The spectrum of the reaction with **4**H_6 exhibits additional signals including an AMX set. The crystals obtained from the solution consist of the complex **4**H$(AlMe_2)_5$. Its pentaanionic ligand $[\mathbf{4}H]^{5-}$ accommodates five $[AlMe_2]^+$ groups; three occupy type **I** chelates in an arrangement equivalent to that of **X''**$H_3(AlMe_2)_3$; the fourth inhabits a bidentate type **III** site while the fifth is found in a type **II** chelate that contains the NH-site. Cooling the solution to 220 K converts the AX_2 to an AMX set in agreement with the molecular symmetry of the crystal structure. The variable temperature study suggests a fluxional behavior that equivalences two P-nuclei in the phosphazene ring (see ESI). Crystallization of the product obtained from the reaction of the ethyl derivative leads to the aggregated complex {**5**H$(AlMe_2)_4\}_2$AlMe. In it two $[\mathbf{5}H(AlMe_2)_4]^-$ fragments are linked via a $[AlMe]^{2+}$ group which occupies the molecular C_2 axis. The coordination pattern is equivalent to that of **4**H$(AlMe_2)_5$, except that in the aggregate the type **II** chelate that contains the NH-site is now binding the bridging $[AlMe]^{2+}$ unit. Remarkably, when crystals of {**5**H$(AlMe_2)_4\}_2$AlMe are re-dissolved, the spectrum of the resulting solution does not produce the AX_2 set that was observed prior to crystallization. Instead it yields an AMX set which is similar to the additional AMX set seen in the spectrum of the reaction of **4**H_6 with five $AlMe_3$. This suggests that the ethyl derivative **5**H$(AlMe_2)_5$ aggregates upon crystallization while the isobutyl derivative aggregates slowly in solution.

When six equivalents $AlMe_3$ are added to **5**H_6 and **6**H_6 at room temperature, the $^{31}P\{^1H\}$ NMR spectra of the reaction mixtures contain a triplet accompanied by a very broad signal. Variable temperature measurements indicate a dynamic process. They show a sharpening of the broad signal into a doublet that becomes part of an AX_2 set upon warming and a splitting into an AMX pattern upon cooling. Crystals grown from the solution contain complexes of composition **5**$(AlMe_2)_6$ and **6**$(AlMe_2)_6$, respectively. The fully deprotonated ligands accommodate six $[AlMe_2]^+$ groups, four in chelates of type **I** and two in chelates of type **III**. These are distributed around the ligand in asymmetric fashion in agreement with the AMX set observed at lower temperature. Considering the coordination pattern of the low temperature form corresponds to that of the crystal structure, a dynamic process that equivalences two P-nuclei in accordance with the AX_2 signal at higher temperature must involve the rearrangement of at least two $[AlMe_2]^+$ groups (Figure 3).

Reactions of **4**H_6 and **8**H_6 reach the fully deprotonated ligand stage only after prolonged refluxing in the presence of six

equivalents $AlMe_3$. This led in both cases to the emergence of a dominant AMX set in the $^{31}P\{^1H\}$ NMR spectrum. Crystals obtained from the reaction solution of the isobutyl derivative contain the complex **4**$(AlMe_2)_6$. It comprises a fully deprotonated ligand accommodating four $AlMe_2$ units in type **I** and two in type **III** chelates. The coordination pattern is very similar to that of **5**$(AlMe_2)_6$ with the only difference that one type **I** chelate has shifted to a neighboring site. The resulting molecular C_2 symmetry varies from the asymmetric structure found in solution. We conclude that either different coordination patterns exist in the crystal and in solution, or that the crystal structure is not representative for the bulk of the compound in solution. The crystal structure of the benzyl derivative exhibits the complex **8**$(AlMe_2)_6$. Its coordination pattern is different to those seen in **4**$(AlMe_2)_6$ and **5**$(AlMe_2)_6$. Three $[AlMe_2]^+$ occupy type **I**, one a type **II** and one a type **III** site, while the remaining group is coordinated to one N(exo) site. In addition, it interacts loosely in side-on fashion with the phenyl ring of a benzyl group. The closest Al...C-contact is towards an ortho-C-atom measuring 267 pm.

The metalation of **7**H_6 was conducted in tetrahydrofuran due to its low solubility in hydrocarbons which can be attributed to its tendency to form dense hydrogen bonding networks.[36] Addition of $AlMe_3$ at room temperature resulted in opaque mixtures that gave only poorly resolved spectra. Refluxing with six equivalents produces a clear solution exhibiting an AMX signal in the $^{31}P\{^1H\}$ NMR spectrum. The crystal structure of the product consists of the dimeric aggregate {**7**$(AlMe_2)_4AlMe\}_2$. The ligands in the centrosymmetric dimer are bridged by two $[AlMe]^{2+}$ groups. They are coordinated by one ligand via a bidentate type **II** site and by the other in monodentate fashion via an N(exo) site. The $[AlMe_2]^+$ groups occupy type **I** and **III** chelates similar as in **4**$(AlMe_2)_6$.

The X-ray structures show that the phosphazene rings are highly distorted in the aluminum complexes. Analysis of ring puckering parameters[37] reveals that the rings adopt twist conformations and become more puckered upon increasing metalation (see ESI). While in **X**H_6 the P-N(ring) bonds are close to 160 pm,[36] they cover an enormous range in the aluminum complexes reaching from 156 to 175 pm. The P-N(exo) bonds exhibit a similar distribution stretching from 157 to 174 pm (see ESI for distribution of P-N bonds). Long P-N bonds occur where either the N-atom binds to two Al-centers or an NH-site is involved in metal coordination. It is remarkable to what extent the P-N(ring) bonds are stretched when compared to other phosphazene species. Some are longer than phosphazene bonds adjacent to alkylated N(ring) sites or phosphate groups.[38-40] They even exceed the bond lengths found in formally saturated cyclophosphazanes[41-45] and phosphazene-phosphazane hybrids.[46-48] The N-P-N angles are equally affected by Al-coordination resulting in severely distorted PN_4 tetrahedra. For example, type **I** and type **II** chelation can reduce the N-P-N angle to below 95°. On the other hand, the average P-N bond lengths per PN_4 tetrahedron are narrowly clustered between 162 and 165 pm (see ESI). This suggests that the strain experienced by the longer P-N bonds is offset by a shortening of neighboring bonds. The ligands have proven to be very robust; degradation of the phosphazene ring was not observed despite the high level of stress put on them.

The Al-N bond lengths show also great variations ranging from 185 to 218 pm. Again, they are long where two Al-centers coordinate to the same nitrogen or one Al interacts with an NH-site. Al-C bonds of $[AlMe_2]^+$ groups average 195 pm in line with the terminal Al-C bonds in the dimer of trimethylaluminum.[49,50] The lengths of Al-C bonds of $[AlMe]^{2+}$ groups are similar: 192.4(3) pm for the group in **3**$(AlMe_2)_4AlMe$; 194.7(4) and 194.8(10) pm for the bridging groups in {**5**$H(AlMe_2)_4\}_2AlMe$ and {**7**$(AlMe_2)_4AlMe\}_2$, respectively. The C-Al-C angles of $[AlMe_2]^+$ groups reflect the interaction with the ligand. They are widest for the monocoordinated group in **8**$(AlMe_2)_6$ (123.33(14)°), followed by the group that occupies the chelate featuring a NH group in **4**$H(AlMe_2)_5$ (120.3(2)°), while groups in bidentate chelates involving pure N-sites range somewhere between 112 and 118°; groups that bind to congested sites tend to be found towards the higher end of this range.

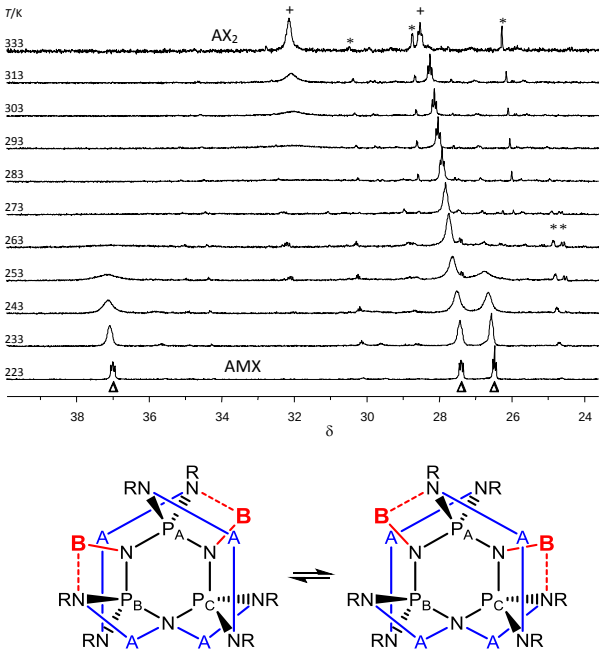

Figure 3. Variable temperature $^{31}P\{^1H\}$ NMR spectra of **5**$(AlMe_2)_6$ in hexane (*denotes impurities). The conversion of the AMX (Δ) into an AX_2 set (+) towards higher temperature indicates a fluxional process that equivalences two of the three P-nuclei in the phosphazene ring. Considering that at low temperature the asymmetric coordination pattern of the crystal is maintained, a viable process that equivalences P_B and P_C would require the re-arrangement of two $[AlMe_2]^+$ groups (A = stationary $[AlMe_2]^+$, B = fluxional $[AlMe_2]^+$). The Al-N bonds that are broken in the process are comparatively long in the crystals (drawn here as dashed lines). The broadening of the signal due to P_A at intermediate temperatures indicates that P_A is also engaged in a dynamic process. This is not a consequence of an exchange with either P_B or P_C as simulations reveal, but may be due to slow adjustment of the quasi-tetrahedral environment around P_A following the re-arrangements of $[AlMe_2]^+$ groups.

DISCUSSION

The study shows that the progress of metalation is finely controlled by the steric demand of the alkyl groups, or more precisely, their level of branching in the vicinity of the N-atom. In the presence of the bulky tert-butyl group the reaction ceases at the dianionic stage at room temperature, while prolonged heating takes it only to the trianionic stage. Derivatives equipped with isopropyl and cyclohexyl groups proceed to the

trianionic stage at room temperature, while refluxing accomplishes full deprotonation. The β-C-branched isobutyl substituent allows the reaction to reach the pentaanionic stage at room temperature, while complete deprotonation is accomplished after reflux. Only ligands carrying small linear ethyl and propyl groups achieve full deprotonation at ambient conditions. Figure 4 illustrates how the steric effect of the R-groups governs the space available for coordination of $[AlMe_2]^+$ and $[AlMe]^{2+}$. It shows that the ligand alkyl and the Al-bound methyl groups form a densely packed spherical shell with an approximate radius of 5 Å around the ligand core. It is also at this distance from the center where α-C-branching of alkyl groups occurs and thus exerts maximum steric effect.

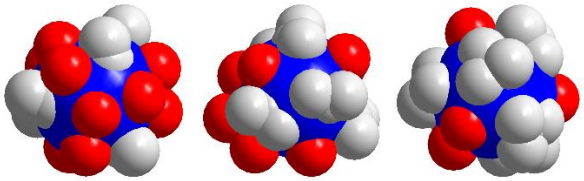

5$(AlMe_2)_6$ **3**$(AlMe_2)_4AlMe$ **1'**$H_3(AlMe_2)_3$

Figure 4. Steric effect of α-C branching at ligand alkyl groups: The ligand alkyl (grey) and Al-bound methyl groups (red) form dense packings around the ligand core on a sphere with a radius of approximately 5 Å (blue). Increased branching of alkyl groups at α-C positions restricts the space available to accommodate additional Al-bound methyl groups. Their highest achievable number decreases from twelve (for R = ethyl in **5**$(AlMe_2)_6$, full metalation is completed at room temperature) to nine (for R = isopropyl in **3**$(AlMe_2)_4AlMe$, full metalation is only accomplished under reflux and integration of the smaller $[AlMe]^{2+}$ group) to six (for R = tert-butyl in **1'**$H_3(AlMe_2)_4AlMe$, the metalation does not progress beyond at the trianionic stage even when refluxed).

The ligands that were observed along the route comprise the dianionic isomer $[\mathbf{X'}H_4]^{2-}$, the two isomers of the trianion $[\mathbf{X'}H_3]^{3-}$ and $[\mathbf{X''}H_3]^{3-}$, the pentaanion $[\mathbf{X}H]^{5-}$ and the hexaanion $[\mathbf{X}]^{6-}$. The perceived absence of the monoanion from the spectra suggests that once it has formed it swiftly reacts to produce $\mathbf{X'}H_4(AlMe_2)_2$. The preference for the dianionic isomer $[\mathbf{X'}H_4]^{2-}$ can be attributed to its non-geminal *trans* configuration which places its two deprotonated N-sites as far apart as possible. Further deprotonation leads to the trianion $[\mathbf{X'}H_3]^{3-}$ if substituents are branched at α-C atoms. With less bulky groups it yields a mixture of isomers $[\mathbf{X'}H_3]^{3-}$ and $[\mathbf{X''}H_3]^{3-}$. Complexes containing trianionic ligands are particularly stable as they offer three separate type **I** chelates. In contrast, the tetraanionic ligand cannot provide four separate chelates without involving NH sites. Considering that Al-coordination will activate the deprotonation of NH-sites, $\mathbf{X}H_2(AlMe_2)_4$ can be deemed more reactive towards $AlMe_3$ than $\mathbf{X}H_3(AlMe_2)_3$ which may explain the more transient existence of the tetraanion. The pentaanion $[\mathbf{X}H]^{5-}$ is the only ligand in this series that coordinates via its NH site while supporting a stable complex. It is less crowded than the hexaanion $[\mathbf{X}]^{6-}$ which may explain its relative stability. For example, while in **4**$H(AlMe_2)_5$ only one N-site is shared between two Al centres, three are shared in **4**$(AlMe_2)_6$. X-ray structures show that Al-N contacts involving shared sites are significantly longer. This suggests that overall coordination is becoming weaker at full metalation.

The metalations follow selective pathways which is remarkable considering the large number of possible ligand isomers and the many ways in which chelating sites can be arranged around them. The high selectivity may be a consequence of the strong interdependence between metal coordination and ligand conformation since chelation locks the orientation of the N-bound steric group and thereby limits the options for metal coordination at neighboring sites. The co-existence of ligand isomers $[\mathbf{X'}H_3]^{3-}$ and $[\mathbf{X''}H_3]^{3-}$ and their direct descendance from the dianionic isomer $[\mathbf{X'}H_4]^{2-}$ (see Scheme 1) suggest that pathways are kinetically controlled to some extent. Fast proton exchange between N-sites can be ruled out in the absence of strongly basic transfer reagents.[10] It is interesting to note that the metalation with n-butyllithium takes a different pathway which proceeds straight to the C_{3v}-symmetric isomer $[\mathbf{X'''}H_3]^{3-}$. It allows the ligand to distribute its negative charge more effectively by distorting into a chair conformation while spreading its deprotonated N-sites along equatorial positions.[10-12] Although $[\mathbf{X'''}H_3]^{3-}$ offers three distinct chelates similar to the other two trianionic isomers, it was not observed in the reactions with trimethylaluminum. The reason may be the lesser ionic character of the aluminum complexes and the lack of a direct deprotonation pathway from the preceding dianionic isomer $[\mathbf{X'}H_4]^{2-}$ (see Scheme 1).

The crystal structures reveal an increasing variety of coordination modes upon progressive metalation. Up to the trianionic stage $[AlMe_2]^+$ groups reside exclusively in separate bidentate type **I** chelates comprising a deprotonated N(exo) and an N(ring) site. Those added at the later stages tend to occupy the more peripheral bidentate type **II** and **III** chelates that have only N(exo) sites. The resulting four- and six-membered metallacycles resemble those found in mononuclear aluminum complexes with ligands containing linear N-P-N and N-P-N-P-N backbones, respectively.[51-53] Monodentate coordination can arise when the ligand becomes highly congested and if additional means of contact are provided, for example in the form of π-donating aryl groups. One such interaction was found in the crystal structure of **8**$(AlMe_2)_6$ where one $[AlMe_2]^+$ group connects to one N(exo)-site and, in addition, makes a loose contact to a phenyl ring. A similar interaction, albeit shorter and intermolecular in nature, was observed in crystals of tribenzylaluminum.[54]

In this series $[AlMe_2]^+$ is the primary product of metalation while $[AlMe]^{2+}$ is produced only at the later stages either to mitigate overcrowding or to facilitate aggregation. Integration of the small and formally dicationic $[AlMe]^{2+}$ unit offsets two deprotonation steps but takes considerably less space than two $[AlMe_2]^+$ groups. This enables full deprotonation of the relatively bulky isopropyl derivative resulting in the pentanuclear complex **3**$(AlMe_2)_4AlMe$. The ligand provides the $[AlMe]^{2+}$ group with a tridentate type **IV** site which supports the familiar tetrahedral coordination environment around the Al-center. The $[AlMe]^{2+}$ group can also bind two ligands and thereby allowing complexes to aggregate. In this way it acts as a bridging unit in $\{\mathbf{7}(AlMe_2)_4AlMe\}_2$ and $\{\mathbf{5}H(AlMe_2)_4\}_2AlMe$. In the latter the bridging Al center is five-coordinate forming two long bonds to NH sites of either ligand. A possible mechanism for the aggregation is the condensation of two $[AlMe_2]^+$ groups. The detection of monomeric **5**$H(AlMe_2)_5$ prior to and aggregated $\{\mathbf{5}H(AlMe_2)_4\}_2AlMe$ after crystallization supports this scenario. In this case, the crystallization brings two complexes into sufficiently close contact to trigger condensation.

Variable temperature NMR studies of **4**H$(AlMe_2)_5$, **5**$(AlMe_2)_6$ and **6**$(AlMe_2)_6$ indicate that fluxional processes can occur during the later stages of metalation (see Figure 3 and ESI). A possible mechanism for this behavior is a dynamic interchange of $[AlMe_2]^+$ groups at crowded N-sites. It is evident from X-ray structures that Al-N bonds are significantly longer when N-sites coordinate to two Al centers. During the interchange one of the Al-N interactions gradually weakens until it breaks. The departing $[AlMe_2]^+$ group then approaches another N-site where it either replaces an existing Al-N interaction or bounces back to its previous position. As a result, $[AlMe_2]^+$ groups will fluctuate between a given set of N-sites. Fluxional behavior was also observed for the bimetallic phosphazenate complex $(PhN)_6P_3N_3H_2AlMe_2Li_3thf_6$. However, in this case the lithium ions oscillate while the $[AlMe_2]^+$ group remained stationary.[55]

CONCLUSION

The study has revealed a multifaceted coordination behavior of $[AlMe_2]^+$ and $[AlMe]^{2+}$ with polyanionic phosphazenates. The polydentate ligands provide a variety of bidentate and tridentate binding pockets; their size is determined by the steric demand of the peripheral sphere of substituents which gives control over the progress of metalation, levels of aggregation and dynamic behavior. While $[AlMe_2]^+$ groups constitute the primary product of the metalation, $[AlMe]^{2+}$ groups are utilized to alleviate overcrowding at spatially restricted sites or to aid aggregation by forming bridges between ligands. At higher grades of metalation $[AlMe_2]^+$ groups can become fluxional, scrambling around congested ligand sites. The ligands proved to be very robust and at the same time extremely flexible offering a unique platform for the exploration of complex multinuclear metal arrangements.

EXPERIMENTAL SECTION

All manipulations were performed under a dry nitrogen atmosphere. Solvents were dried over potassium (thf, hexane) and sodium (toluene). Precursors **X**H_6 were prepared as reported previously[36] apart from **5**H_6, which is described in here. Trimethylaluminum (2.0 M in hexane) was purchased from Aldrich and used as received. FT-IR spectra were recorded on a Perkin-Elmer Paragon 1000 spectrometer in nujol between CsI plates. NMR spectra were recorded on a Bruker AMX 400 spectrometer (^{1}H NMR: 400.13 MHz, $^{13}C\{^1H\}$ NMR: 100.62 MHz, $^{31}P\{^1H\}$ NMR: 161.97 MHz) at room temperature (if not stated otherwise) in C_6D_6 using $SiMe_4$ (^{1}H, ^{13}C) and 85% H_3PO_4 (^{31}P) as external standards.

Single crystal X-ray structure analysis was carried out using MoK_α radiation (λ = 0.71073 Å). Crystal structures were refined with full-matrix least-squares against F^2 using all data (crystallographic tables are found in the ESI).[56] CCDC deposition numbers are as follows: **1**'$H_4(AlMe_2)_2$, CCDC 1881689; **1**'$H_3(AlMe_2)_3$, CCDC 1881692; **2**'$H_3(AlMe_2)_3$, CCDC 1881690; **3**$(AlMe_2)_4AlMe$, CCDC 1881691; **4**H$(AlMe_2)_5$, CCDC 1881696; **4**$(AlMe_2)_6$, CCDC 1881695; {**5**H$(AlMe_2)_4\}_2AlMe$, CCDC 1881694; **5**$(AlMe_2)_6$, CCDC 1881688; **6**$(AlMe_2)_6$, CCDC 1881697; {**7**$(AlMe_2)_4AlMe\}_2$, CCDC 1881698; **8**$(AlMe_2)_6$, CCDC 1881693; **5**H_6, CCDC 1881699.

1'$H_4(AlMe_2)_2$: 1.76 mL (3.52 mmol) $AlMe_3$ (2.0 M in hexane) was added to 1.00 g (1.76 mmol) **1**H_6 in 10 mL of hexane. The solution was stirred for 1 h, filtered and then reduced to 2 mL. Colorless crystals formed at 5˚C overnight. Yield 0.93 g (78%). ^{1}H NMR δ -0.5 - -0.2 [m, 12H, AlMe], 1.27 - 1.42 [m, 54H, tBu], 2.08 [m, 4H, NH]. $^{13}C\{^1H\}$ NMR δ 19 [m, C(CH_3)$_3$], 30 [m, $C(CH_3)_3$]. $^{31}P\{^1H\}$ NMR δ 5.6 [t, $^2J_{P\text{-}P}$ = 44 Hz], 8.3 [d, $^2J_{P\text{-}P}$ = 44Hz]. IR ν (cm^{-1}) 1263, 1224, 1184, 1022 (P-N), 989, 891, 861, 805, 626.

1'H_3 $(AlMe_2)_3$: 2.64 mL (5.28 mmol) $AlMe_3$ (2.0 M in hexane) was added to 1.00 g (1.76 mmol) **1**H_6 in 20 mL of hexane. The solution was refluxed for 1 h, filtered and then reduced to 2 mL. Colorless crystals formed from a mixture of hexane and toluene after a few days at room temperature. Yield 0.93 g (72%). ^{1}H NMR δ -0.4 - -0.2 [m, 18H, AlMe], 1.2 - 1.5 [m, 54H, *t*Bu], 2.0 - 2.1 [m, 3H, NH]. $^{13}C\{^1H\}$ NMR δ -2 [m, AlMe], 32 (m, C(CH_3)$_3$), 51 (m, $C(CH_3)_3$). $^{31}P\{^1H\}$NMR δ 2.3 [dd, $^2J_{P\text{-}P}$, 24 Hz and 5 Hz], 4.83 [dd, $^2J_{P\text{-}P}$ = 24 and 18 Hz], 7.2 [dd, $^2J_{P\text{-}P}$ = 18 and 5 Hz]. IR ν (cm^{-1}) 1260, 1229, 1192, 1148, 1080 (P-N), 1042 (P-N), 1020 (P-N), 906, 813, 754, 672, 613.

2'$H_3(AlMe_2)_3$: 2.02 mL (4.14 mmol) $AlMe_3$ (2.0 M in hexane) was added to 1.00 g (1.38 mmol) **2**H_6 in 20 mL of hexane. The solution was stirred for 1 h, filtered and then reduced to 2 mL. Colorless crystals formed at 5˚C overnight. Yield 0.92 g (75%). ^{1}H NMR δ -0.2 - -0.1 [m, 18H, AlMe], 1.0 - 2.6 [m, 60H, Cy], 3.2 - 3.5 [m, 6H, NCH_2]. $^{13}C\{^1H\}$ NMR δ -7 [m, AlMe], 26, 37, 50, 68 [m, Cy]. $^{31}P\{^1H\}$ NMR δ 9.9 [dd, $^2J_{P\text{-}P}$ = 19 Hz and 4 Hz], 13.0 [dd, $^2J_{P\text{-}P}$ = 19 Hz and 16 Hz], 16.6 [dd, $^2J_{P\text{-}P}$ = 16 and 4 Hz]. IR ν (cm^{-1}) 1293, 1260, 1191, 1095 (P-N), 1022 (P-N), 956, 848, 815, 713, 668.

3'$H_3(AlMe_2)_3$: 2.07 mL (6.21 mmol) $AlMe_3$ (2.0 M in hexane) was added to 1.00 g (2.07 mmol) **3**H_6 in 20 mL of hexane. The solution was stirred for 1 h, filtered and then reduced to 2 mL. Colorless crystals formed at 5˚C overnight. Yield 1.20 g (89%). ^{1}H NMR δ -0.1 - -0.3 [m, 18H, AlMe], 1.1 - 1.7 [m, 36H, CH(CH_3)$_2$], 3.6 - 3.8 [m, 6H, $CH(CH_3)_2$], 3.58 [m, 3H, NH]. $^{13}C\{^1H\}$ NMR δ 2 [m, AlMe], 26 [m, $CH(CH_3)_2$], 46 [m, $CH(CH_3)_2$]. $^{31}P\{^1H\}$ NMR δ 9.1 [dd, $^2J_{P\text{-}P}$ 22 and 3 Hz], 12.7 [dd, $^2J_{P\text{-}P}$ = 22 and 17 Hz], 15.9 [dd, $^2J_{P\text{-}P}$ = 17 and 3 Hz]. IR ν (cm^{-1}) 1303, 1222, 1189, 1081 (P-N), 1035 (P-N), 934, 863, 786, 707, 675.

3$(AlMe_2)_4AlMe$: 2.64 mL (10.35) $AlMe_3$ (2.0 M in hexane) was added to 1.00 g (2.07 mmol) **3**H_6 in 20 mL of hexane. The solution was refluxed for 3 h, filtered and then reduced to 10 mL. Colorless crystals formed at 5˚C overnight. Yield 1.41 (91%). ^{1}H NMR δ -0.2 - 0.1 [m, 27H, AlMe],1.2 - 1.6 [m, 36H, CH(CH_3)$_2$], 3.5 - 4.0 [m, 6H, $CH(CH_3)_2$]. $^{13}C\{^1H\}$ NMR δ -4 [m, $(CH_3)_2Al$], 29 [m, $CH(CH_3)_2$], 46, [m, $CH(CH_3)_2$]. $^{31}P\{^1H\}$ NMR δ 12.6 [dd, $^2J_{P\text{-}P,}$ 11 and 3 Hz], 15.6 [dd, $^2J_{P\text{-}P,}$ 9 and 3 Hz], 16.8, [dd, $^2J_{P\text{-}P,}$ 11 and 9 Hz]. IR ν (cm^{-1}) 1190, 1158, 1108 (P-N), 1084 (P-N), 1051 (P-N), 1008, 929, 905, 864, 850, 826, 809, 784, 712.

4H$(AlMe_2)_5$: 4.40 mL (8.80 mmol) $AlMe_3$ (2.0 M in hexane) was added to 1.00 g (1.76 mmol) **4**H_6 in 20 mL of hexane. The solution was stirred for 1 h followed by 15 min. reflux, filtered and then reduced to 10 mL. Colorless crystals formed after a few days storage at room temperature. Yield (1.28 g) 86%. ^{1}H NMR δ = -0.6 - -0.2 [m, 30H, AlMe], 0.7 - 1.0 [m, 36H, $CH_2CH(CH_3)_2$], 1.6 - 1.8 [m, 6H, $CH_2CH(CH_3)_2$], 2.7 - 3.2 [m, 12H, $CH_2CH(CH_3)_2$]. $^{13}C\{^1H\}$ NMR δ -6 [m, AlMe], 21 [m, $CH_2CH(CH_3)_2$], 30 [m, $CH_2CH(CH_3)_2$], 51 [m, $CH_2CH(CH_3)_2$]. $^{31}P\{^1H\}$ NMR δ 16.9 [t, $^2J_{P\text{-}P}$ = 8 Hz], 28.6 [d, $^2J_{P\text{-}P}$ = 8 Hz], at 213 K: δ 15.1 [dd, $^2J_{P\text{-}P}$ = 9 and 8 Hz] , 27.0 [dd, $^2J_{P\text{-}P}$ = 9 and < 1 Hz], 28.4 [dd, $^2J_{P\text{-}P}$ = 8 and < 1 Hz]. IR ν (cm^{-1}) 1256, 1198, 1084 (P-N), 1043 (P-N), 998, 944, 876, 799, 699.

4$(AlMe_2)_6$: 5.37 mL (10.56 mmol) $AlMe_3$ (2.0 M in hexane) was added to 1.00 g (1.76 mmol) **4**H_6 in 20 mL of hexane. The solution was refluxed for 24 h, filtered and then reduced to 10 mL. Colorless crystals formed at 5˚C overnight. Yield 1.19 g (75%). ^{1}H NMR δ -0.8 - -0.3 [m, 36H, AlMe], 0.6 - 1.0 [m, 18H, $CH_2CH(CH_3)_2$], 1.4 - 1.7 [m, 12H, $CH_2CH(CH_3)_2$], 2.4 - 2.8 [m, 12H, $CH_2CH(CH_3)_2$]. $^{13}C\{^1H\}$ NMR δ -8 [m, AlMe], 12 [m, $CH_2CH(CH_3)_2$], 25 [m, $CH_2CH(CH_3)_2$], 41 [m, $CH_2CH(CH_3)_2$]. $^{31}P\{^1H\}$ NMR δ 20.3, 24.8, 28.7 [$^2J_{P\text{-}P}$ < 1 Hz]. IR ν (cm^{-1}) 1262, 1194, 1107 (P-N), 1071 (P-N), 1034 (P-N), 980, 944, 858, 799, 685.

{**5**H$(AlMe_2)_4\}_2AlMe$: 6.23 mL (12.50 mmol) $AlMe_3$ (2.0 M in hexane) was added to 1.00 g (2.50 mmol) **5**H_6 in 20 mL of hexane. The solution was stirred for 1 h. Colorless crystals formed at 5˚C overnight. Yield 0.85 g (53%). ^{1}H NMR δ -0.7 - -0.4 [m, 51H, AlMe], 0.6 - 1.1 [m, 36H, CH_2CH_3], 2.6 - 3.0 [m, 24H, CH_2CH_3]. $^{13}C\{^1H\}$ NMR δ -5 [m, 17C, AlMe], 17 [m, 6C, CH_2CH_3], 38 [m, 6C, CH_2CH_3]. $^{31}P\{^1H\}$ NMR δ 26.5 [dd, $^2J_{P\text{-}P}$ = 20 and < 1 Hz], 31.3 [dd, $^2J_{P\text{-}P}$ = 20 and 15 Hz], 32.0 [dd, $^2J_{P\text{-}P}$ = 15 and < 1 Hz]. IR ν (cm^{-1}) 1298, 1190, 1101 (P-N), 1069 (P-N), 1043 (P-N), 993, 881, 707, 680.

5$(AlMe_2)_6$: 7.64 mL (15.00 mmol) $AlMe_3$ (2.0 M in hexane) was added to 1.00 g (2.50 mmol) **5**H_6 in 20 mL of hexane. The solution was refluxed for 1 h, filtered and reduced to 10 mL. Colorless crystals formed at 5˚C overnight. Yield 1.53 g (83%). ^{1}H NMR δ -0.7 - -0.5 [s, 36H, AlMe], 0.6 - 0.9 [m, 18H, CH_2CH_3], 2.5 - 2.9 [m, 12H, CH_2CH_3]. $^{13}C\{^1H\}$ NMR δ -6 [m, AlMe], 16 [m, CH_2CH_3], 38 [m, CH_2CH_3]. $^{31}P\{^1H\}$ NMR δ 28.1 [t, $^2J_{P-P}$ = 8 Hz], 32.0 [br]; at 223 K: δ 26.5 [dd, $^2J_{P-P}$ = 7 and 8 Hz], 27.4 [dd, $^2J_{P-P}$ = 11 and 7 Hz], 37.0 [dd, $^2J_{P-P}$ = 11 and 8 Hz]. IR ν (cm^{-1}) 1202, 1175, 1098 (P-N), 1039 (P-N), 998, 944, 908, 849, 708, 667.

6$(AlMe_2)_6$: 6.21 mL (12.42 mmol) $AlMe_3$ (2.0 M in hexane) was added to 1.00 g (2.07 mmol) **6**H_6 in 20 mL of hexane. The solution was refluxed for 2 h, filtered and then reduced to 10 mL. Colorless crystals formed at 5˚C overnight. Yield 1.51g (89%). ^{1}H NMR δ -0.6 - -0.1 [m, 36H, AlMe], 0.7 - 1.0 [m, 18H, $CH_2CH_2CH_3$], 1.4 - 1.5 [m, 12H, $CH_2CH_2CH_3$], 3.0 - 3.3 [m, 12H, $CH_2CH_2CH_3$]. $^{13}C\{^1H\}$ NMR δ -6 [m, 12C, AlMe], 10 [m, $CH_2CH_2CH_3$], 28 [m, $CH_2CH_2CH_3$], 42 [m, $CH_2CH_2CH_3$]. $^{31}P\{^1H\}$ NMR δ 27.3 [t, $^2J_{P-P}$ = 9 Hz], 31.8 [br]; at 213 K: δ 26.3 [dd, $^2J_{P-P}$ = 11 and 7 Hz], 26.7 [dd, $^2J_{P-P}$ = 8 and 7 Hz], 36.2 [dd, $^2J_{P-P}$ = 11 and 8 Hz]; at 233 K: δ 27.9 [t, $^2J_{P-P}$ = 8 Hz], 31.9 [dd, $^2J_{P-P}$ = 8 Hz]. IR ν (cm^{-1}) 1313, 1259, 1201, 1094 (P-N), 1032 (P-N), 952, 903, 845, 805, 685.

{**7**$(AlMe_2)_4AlMe\}_2$: 9.67 mL (19.) $AlMe_3$ (2.0 M in hexane) was added to a suspension of 1.00 g (3.17 mmol) **7**H_6 in 20 mL of thf. The solution was refluxed for 1 h and filtered. Colorless crystals were obtained from toluene at 5˚C overnight. Yield 1.43 g (78%). ^{1}H NMR δ -0.8 - -0.4 [m, 54H, AlMe], 1.8 - 2.5 [m, 36H, NMe]. $^{13}C\{^1H\}$ NMR δ = -9 [m, AlMe], 30 [m, NMe]. $^{31}P\{^1H\}$ NMR δ 37.9, 34.3, 24.9 [$^2J_{P-P}$ < 1 Hz]. IR ν (cm^{-1}) 1256, 1193, 1084 (P-N stretch), 1021 (P-N stretch), 930, 853, 803, 686.

8$(AlMe_2)_6$: 3.90 mL (7.80 mmol) $AlMe_3$ (2.0 M in hexane) was added to 1.00 g (1.30 mmol) **8**H_6 in 20 mL of hexane. The solution was reflux for 24 h, filtered and reduced to 10 mL. Colorless crystals formed at 5˚C overnight. Yield 1.16 g (81%). ^{1}H NMR δ -0.5 - -0.1 [m, 36H, AlMe], 3.4 - 5.3 [m, 12H, NCH_2], 6.6 - 8.1 [m, 30H, Ph]. $^{13}C\{^1H\}$ NMR δ = -9 [m, AlMe], 58 [m, 12H, NCH_2], 132 - 139 [m, 12H, Ph]. $^{31}P\{^1H\}$ NMR δ 40.1, 25.6, 20.2 [$^2J_{P-P}$ < 1 Hz]. IR ν (cm^{-1}) 1260, 1194, 1110, 1073 (P-N), 1042 (P-N), 1026 (P-N), 942, 796, 697.

5H_6: To a stirred solution of 10 g (28.8 mmol) hexachlorocyclotriphosphazene in 200 ml of toluene were added 50 mL (358 mmol) triethylamine followed by 16 g (355 mmol) ethylamine. Precipitation of hydrochloride salts indicated the onset of the reaction. After the mixture was stirred for 24 h all volatiles were removed in vacuo. A suspension of 15 g finely ground KOH in 150 mL diethylether was added to the residue. The mixture was stirred for 12 h after which all volatiles were removed in vacuo. The product was extracted from the residue by Soxhlet extraction with toluene (24 h). Yield 7.1 g (62%). Colorless single crystals suitable for X-ray structure determination were obtained by slow cooling from the melt (m.p.: 105-107°C). ^{1}H NMR ($CDCl_3$) δ 1.04 (t, 18H, CH_2CH_3, $^3J_{H-H}$ = 7.2 Hz), 1.97 (br, 6H, NH), 2.88 (d, 12H, CH_2CH_3, $^3J_{H-H}$ = 7.2 Hz). $^{13}C\{^1H\}$ NMR ($CDCl_3$) δ 16.5 (s, 6C, CH_2CH_3), 34.6 (s, 6C, CH_2CH_3). $^{31}P\{^1H\}$ NMR (toluene d_8) δ 18.2 (s). IR ν (cm^{-1}) 1183 (P-N), 1120 (P-N), 1069 (P-N), 951, 880, 850, 812, 749, 715.

ASSOCIATED CONTENT

Supporting Information

The Supporting Information is available free of charge on the ACS Publications website.

$^{31}P\{^1H\}$ NMR spectra of sequential additions and variable temperature measurements, tables with crystallographic data, analysis of ring puckering parameters and distribution of P-N and Al-N bond lengths (PDF)

Accession Codes

CCDC 1881688-1881699 contain the supplementary crystallographic data for this paper. These data can be obtained free of charge via www.ccdc.cam.ac.uk/data_request/cif, or by emailing data_request@ccdc.cam.ac.uk, or by contacting The Cambridge Crystallographic Data Centre, 12 Union Road, Cambridge CB2 1EZ, UK; fax: +44 1223 336033.

AUTHOR INFORMATION

Corresponding Author

* Email: a.steiner@liv.ac.uk

Notes

The authors declare no competing financial interest.

ORCID

Alexander Steiner: 0000-0002-4315-6123

Craig M. Robertson: 0000-0002-4789-7607

ACKNOWLEDGMENT

This work was supported by EPSRC.

DEDICATION

Dedicated to Prof. Dr. Dietmar Stalke on the occasion of his 60th birthday

REFERENCES

(1) Chandrasekhar, V.; Nagendran, S. Phosphazenes as Scaffolds for the Construction of Multi-Site Coordination Ligands, *Chem. Soc. Rev.* **2001**, *30*, 193-203.

(2) Steiner, A.; Zacchini, S.; Richards, P. I. From Neutral Iminophosphoranes to Multianionic Phosphazenates. The Coordination Chemistry of Imino–aza-P (V) Ligands, *Coord. Chem. Rev.* **2002**, *227*, 193-216.

(3) Chandrasekhar, V.; Thilagar, P.; Pandian, B. M. Cyclophosphazene-Based Multi-Site Coordination Ligands *Coord. Chem. Rev.* **2007**, *251*, 1045-1074.

(4) Steiner, A.; Wright, D. S. Hexalithiated Hexakis(cyclohexylamino)-Cyclotriphosphazene; a $(Li^+)_{12}$ Cage Containing Puckered $[NP(NCy)_2]_3^{6-}$ Ions, *Angew. Chem. Int. Ed.* **1996**, *35*, 636-637.

(5) Boomishankar, R.; Richards, P. I.; Gupta, A. K.; Steiner, A. Magnesium and Titanium Complexes of Polyanionic Phosphazenate Ligands, *Organometallics* **2010**, *29*, 2515-2520.

(6) Lawson, G. T.; Jacob, C.; Steiner, A. Organometallic Complexes of Multianionic Phosphazenates, *Eur. J. Inorg. Chem.* **1999**, 1881-1887.

(7) Rivals, F.; Steiner, A. The Pentadecadentate Phosphazenate $[\{2\text{-}(MeO)C_6H_4N\}_6P_3N_3]^{6-}$: Chelation of Twelve Lithium Ions by a Single Ligand, *Chem. Commun.* **2001**, 1426-1427.

(8) Boomishankar, R.; Richards, P. I.; Steiner, A. Tris(organozinc) Phosphazenates as Templates for Trimeric and Hexameric Zinc Oxide Clusters, *Angew. Chem. Int. Ed.* **2006**, *45*, 463-4634.

(9) Richards, P. I.; Boomishankar, R.; Steiner, A. Zinc Oxide Clusters Encapsulated by Organozinc Phosphazenate Assemblies, *J. Organomet. Chem.* **2007**, *692*, 2773-2779.

(10) Lawson, G. T.; Rivals, F.; Tascher, M.; Jacob, C.; Bickley, J. F.; Steiner, A. cis-Trihydrogen Cyclotriphosphazenates - Acidic Anions in Strongly Basic Media, *Chem. Commun.* **2000**, 341-342.

(11) Rivals, F.; Lawson, G. T.; Benson, M. A.; Richards, P. I.; Zacchini, S.; Steiner, A. Lithium Complexes of Tri- and Hexaanionic Cyclophosphazenates, the Impact of Metal Coordination on the Ring Conformation, *Inorg. Chim. Acta* **2011**, *372*, 304-312.

(12) Rivals, F.; Steiner, A. Syntheses and Structures of Trilithium Cyclotriphosphazenates Equipped with 2-Halo-aryl Substituents, *Z. Anorg. Allg. Chem.* **2003**, *629*, 139-146.

(13) Dagorne, S.; Atwood, D. A. Synthesis, Characterization, and Applications of Group 13 Cationic Compounds, *Chem. Rev.* **2008**, *108*, 4037-4071.

(14) Sarazin, Y.; Carpentier, J.-F. Discrete Cationic Complexes for Ring-opening Polymerization Catalysis of Cyclic Esters and Epoxides, *Chem. Rev.* **2015**, *115*, 3564-3614.

(15) Wei, Y.; Wang, S.; Zhou, S. Aluminum Alkyl Complexes: Synthesis, Structure, and Application in ROP of Cyclic Esters, *Dalton Trans.* **2016**, *45*, 4471-4485.

(16) Tebbe, F. N.; Parshall, G. W.; Reddy, G. S. Olefin Homologation with Titanium Methylene Compounds, *J. Am. Chem. Soc.* **1978**, *100*, 3611-3613.

(17) Knochel, P.; Blümke, T.; Groll, K.; Chen, Y. H. Preparation of Organoalanes for Organic Synthesis, *Top. Organomet. Chem.* **2013**, *41*, 173-186.

(18) von Zezschwitz, P. Organoaluminum Couplings to Carbonyls, Imines, and Halides, *Top. Organomet. Chem.* **2013**, *41*, 245-276.

(19) Mahalakshmi, L.; Stalke, D. The R_2M^+ Group 13 Organometallic Fragment Chelated by P-Centered Ligands, *Struct. Bonding* **2002**, *103*, 85-115.

(20) Zurek, E.; Ziegler, T. Theoretical Studies of the Structure and Function of MAO (Methylaluminoxane), *Prog. Polym. Sci.* **2004**, *29*, 107-148.

(21) Kaminsky, W. Discovery of Methylaluminoxane as Cocatalyst for Olefin Polymerization, *Macromolecules* **2012**, *45*, 3289-3297.

(22) Chen, E. Y.-X.; Marks, T. J. Cocatalysts for Metal-Catalyzed Olefin Polymerization: Activators, Activation Processes, and Structure-Activity Relationships, *Chem. Rev.* **2000**, *100*, 1391-1434.

(23) Zijlstra, H. S.; Harder, S. Methylalumoxane–History, Production, Properties, and Applications, *Eur. J. Inorg. Chem.* **2015**, 19-43.

(24) Linnolahti, M.; Collins, S. Formation, Structure, and Composition of Methylaluminoxane, *ChemPhysChem* **2017**, *18*, 3369-3374.

(25) Harlan, C. J.; Bott, S. G.; Barron, A. R. Three-Coordinate Aluminum Is Not a Prerequisite for Catalytic Activity in the Zirconocene-Alumoxane Polymerization of Ethylene, *J. Am. Chem. Soc.* **1995**, *117*, 6465-6474.

(26) Jones, A. C.; Rushworth, S. A.; Houlton, D. J.; Roberts, J. S.; Roberts, V.; Whitehouse, C. R.; Critchlow, G. W. Deposition of Aluminum Nitride Thin Films by MOCVD from the Trimethylaluminum–Ammonia Adduct, *Chem. Vap. Deposition* **1996**, *2*, 5-8.

(27) Groner, M. D.; Fabreguette, F. H.; Elam, J. W.; George, S. M. Low-Temperature Al_2O_3 Atomic Layer Deposition, *Chem. Mater.* **2004**, *16*, 639-645.

(28) Watson, I. M. Metal Organic Vapour Phase Epitaxy of AlN, GaN, InN and their Alloys: A key Chemical Technology for Advanced Device Applications, *Coord. Chem. Rev.* **2013**, *257*, 2120-2141.

(29) Kukli, K.; Ritala, M.; Pore, V.; Leskelä, M.; Sajavaara, T.; Hegde, R. I.; Gilmer, D. C.; Tobin, P. J.; Jones, A. C.; Aspinall, H. C. Atomic Layer Deposition and Properties of Lanthanum Oxide and Lanthanum Aluminum Oxide Films, *Chem. Vap. Deposition*, **2006**, *12*, 158-164.

(30) Harrison-Marchand, A.; Mongin, F. Mixed AggregAte (MAA): A Single Concept for All Dipolar Organometallic Aggregates. 1. Structural Data, *Chem. Rev.* **2013**, *113*, 7470-7562.

(31) Mason, M. R.; Smith, J. M.; Bott, S. G.; Barron, A. R. Hydrolysis of Tri-tert-butylaluminum: the First Structural Characterization of Alkylalumoxanes $[(R_2Al)_2O]_n$ and $(RAlO)_n$, *J. Am. Chem. Soc.* **1993**, *115*, 4971-4984.

(32) Harlan, C. J.; Mason, M. R.; Barron, A. R. tert-Butylaluminum Hydroxides and Oxides: Structural Relationship between Alkylalumoxanes and Alumina Gels, *Organometallics* **1994**, *13*, 2957-2969.

(33) Waggoner, K. M.; Power, P. P. Reactions of Trimethylaluminum or Trimethylgallium with Bulky Primary Amines: Structural Characterization of the Thermolysis Products, *J. Am. Chem. Soc.* **1991**, *113*, 3385-3393.

(34) Smith, J. M.; Bott, S. G. A Pentaaluminium Complex of Calix[6]arene: a Bulky Ligand that is Sterically Undemanding, *Chem. Commun.* **1996**, 377-378.

(35) Atwood, J. L.; Gardiner, M. G.; Jones, C.; Raston, C. L.; Skelton, B. W.; White, A. H. Trimethyl-Aluminium and -Gallium Derivatives of Calix[4]arenes: Cone (Monometallic) or Doubly Flattened Partial Cone (tetrametallic) Conformations, *Chem. Commun.* **1996**, 2487-2488.

(36) Bickley, J. F.; Bonar-Law, R.; Lawson, G. T.; Richards, P. I.; Rivals, F.; Steiner, A.; Zacchini, S. Supramolecular Variations on a Molecular Theme: The Structural Diversity of Phosphazenes $(RNH)_6P_3N_3$ in the Solid State, *Dalton Trans.* **2003**, 1235-1244.

(37) Cremer, D.; Pople, J. A. General Definition of Ring Puckering Coordinates, *J. Am. Chem. Soc.* **1975**, *97*, 1354-1358.

(38) Benson, M. A.; Zacchini, S.; Boomishankar, R.; Chan, Y.; Steiner, A. Alkylation and Acylation of Cyclotriphosphazenes, *Inorg. Chem.* **2007**, *46*, 7097-7108.

(39) Benson, M. A.; Ledger, J.; Steiner A. Zwitterionic Phosphazenium Phosphazenate Ligands, *Chem. Commun.* **2007**, 3823-3825

(40) Ledger, J.; Boomishankar, R.; Steiner, A. Aqueous Chemistry of Chlorocyclophosphazenes: Phosphates $\{PO_2\}$, Phosphamides {P(O)NHR}, and the first Phosphites {PHO} and Pyrophosphates $\{(PO)_2O\}$ of These Heterocycles, *Inorg. Chem.* **2010**, *49*, 3896-3904.

(41) Stahl, L. Bicyclic and Tricyclic Bis(amido)cyclodiphosph(III)azane Compounds of Main Group Elements, *Coord. Chem. Rev.* **2000**, *210*, 203-250.

(42) Gonzalez-Calera, S.; Wright, D. S. Macrocyclic Phosphazane Ligands, *Dalton Trans.* **2010**, *39*, 5055-5065

(43) Balakrishna, M. S.; Eisler, D. J.; Chivers, T. Chemistry of Pnictogen(III)–Nitrogen Ring Systems, *Chem. Soc. Rev.* **2007**, *36*, 650-664.

(44) Balakrishna, M. S. Cyclodiphosphazanes: Options are Endless, *Dalton Trans.* **2016**, *45*, 12252-12282.

(45) Shi, Y. X.; Xu, K.; Clegg, J. K.; Ganguly, R.; Hirao, H.; Friscic, T.; Garcia, F. The First Synthesis of the Sterically Encumbered Adamantoid Phosphazane $P_4(NtBu)_6$: Enabled by Mechanochemistry, *Angew. Chem. Int. Ed.* **2016**, *55*, 12736-12740.

(46) Besli, S.; Coles, S. J.; Davies, D. B.; Erkovan, A. O.; Hursthouse, M. B.; Kilic, A. Stable P-N Bridged Cyclophosphazenes with a Spiro or Ansa Arrangement, *Inorg. Chem.* **2008**, *47*, 5042-5044.

(47) Besli, S.; Mutlu, C.; Ibisoğlu, H.; Yuksel, F.; Allen, C. W. Synthesis of a New Class of Fused Cyclotetraphosphazene Ring Systems, *Inorg. Chem.* **2015**, *54*, 334-341.

(48) Richards, P. I.; Steiner, A. A Spirocyclic System Comprising Both Phosphazane and Phosphazene Rings, *Inorg. Chem.* **2005**, *44*, 275-281.

(49) Lewis, P. H.; Rundle, R. E. Electron Deficient Compounds. VII. The Structure of the Trimethylaluminum Dimer, *J. Chem. Phys.* **1953**, *21*, 986-992.

(50) Stammler, H.-G.; Blomeyer, S.; Berger, R. J. F.; Mitzel, N. W. Trimethylaluminum: Bonding by Charge and Current Topology, *Angew. Chem. Int. Ed.* **2015**, *54*, 13816-13820.

(51) Witt, M.; Roesky, H. W. Transition and Main Group Metals in Cyclic Phosphazanes and Phosphazenes, *Chem. Rev.* **1994**, *94*, 1163-1181.

(52) Prashanth, B.; Singh, S. A New Bulky Iminophosphonamide as an N, N′-Chelating Ligand: Synthesis and Structural Characterization of Heteroleptic Group 13 Element Complexes, *Dalton Trans.* **2014**, *43*, 16880-16888.

(53) Jaiswal, K.; Prashanth, B.; Bawari, D.; Singh, S. Bis (phosphinimino) amide Supported Borondihydride and Heteroleptic Dihalo Compounds of Group 13, *Eur. J. Inorg. Chem.* **2015**, 2565-2573.

(54) Rahman, A. F. M. M.; Siddiqui, K. F.; Oliver, J. P. Crystal and Molecular Structure of Tribenzylaluminum, a Novel η^1-Arene Coordinated Structure, *Organometallics* **1982**, *1*, 881-883.

(55) Rivals, F.; Steiner, A. Synthesis and Structure of $[\{(THF)_2Li\}_3Me_2Al\{(PhNH)_2(PhN)_4P_3N_3\}]$, the First Mixed-Metal Phosphazenate Complex, *Eur. J. Inorg. Chem.* **2003**, 3309-3313.

(56) Sheldrick, G. M. A short history of SHELX, *Acta Crystallogr. Sect. A* **2008**, *64*, 112-122.